

There is a short gamma-ray burst prompt phase at the beginning of each long one

G. Calderone^{1*}, G. Ghirlanda¹, G. Ghisellini¹, M. G. Bernardini¹, S. Campana¹, S. Covino¹, D’Avanzo¹, V. D’Elia^{2,3}, A. Melandri¹, R. Salvaterra⁴, B. Sbarufatti^{5,1}, G. Tagliaferri¹

¹*INAF-Osservatorio Astronomico di Brera, via E. Bianchi 46, I-23807 Merate (LC), Italy*

²*ASI-Science Data Centre, Via del Politecnico snc, I-00133 Rome, Italy*

³*INAF-Osservatorio Astronomico di Roma, via Frascati 33, I-00040 Monteporzio Catone (RM), Italy*

⁴*INAF-IASF Milano, via E. Bassini 15, I-20133, Milano, Italy*

⁵*Department of Astronomy and Astrophysics, Pennsylvania State University, University Park, PA, 16802, USA*

13 November 2021

ABSTRACT

We compare the prompt intrinsic spectral properties of a sample of short Gamma-ray Bursts (GRBs) with the first 0.3 seconds (rest frame) of long GRBs observed by *Fermi*/GBM. We find that short GRBs and the first part of long GRBs lie on the same E_p - E_{iso} correlation, that is parallel to the relation for the time averaged spectra of long GRBs. Moreover, they are indistinguishable in the E_p - L_{iso} plane. This suggests that the emission mechanism is the same for short and for the beginning of long events, and both short and long GRBs are very similar phenomena, occurring on different timescales. If the central engine of a long GRB would stop after $\sim 0.3 \times (1+z)$ seconds the resulting event would be spectrally indistinguishable from a short GRB.

Key words: gamma-ray burst: general

1 INTRODUCTION

Gamma-ray bursts (GRBs) are transient emission episodes of radiation detected at high energies. The first emission phase, detected at hard X-rays and γ -rays, lasts for ~ 0.01 ms–100 s (prompt phase). Then, the bulk of emitted radiation shifts to lower energies and becomes observable at longer wavelengths, from X-rays to radio, with typical duration of \sim days–months (afterglow phase). The observed duration of the prompt phase is characterised by the T_{90} parameter, i.e. the time interval during which the central 90% of the counts are recorded by the detector. The distribution of T_{90} of GRBs observed by the Burst And Transient Source Experiment (BATSE) on board the Compton Gamma Ray Observatory (*CGRO*) has been found to be bimodal with a separation at ~ 2 s in the observer frame (Kouveliotou et al. 1993). According to this finding, GRBs are classified either as *short* gamma-ray burst (SGRB) if $T_{90} < 2$, or as *long* ones (LGRB) if $T_{90} > 2$ s (but see Bromberg et al. 2013). Besides, the prompt phase of SGRBs is characterised by harder spectra (Kouveliotou et al. 1993) and smaller spec-

tral lags between different energy bands (Norris et al. 2000) with respect to the prompt phase of LGRBs.

For bursts with reliable redshift estimates, it has been shown that SGRBs are systematically less energetic than LGRBs, with total X and γ -ray emitted energies smaller by a factor ~ 10 –100 (Ghirlanda et al. 2009). Also, the afterglows of SGRBs, when detected, are correspondingly dimmer than those of LGRBs, but similar in other respects (Gehrels et al. 2008; Margutti et al. 2013; D’Avanzo et al. 2014). Finally, several nearby ($z < 0.5$) long GRBs have been associated with explosions of core-collapse supernovae (Hjorth & Bloom 2012), while there is no similar evidence for short bursts (Berger 2013). These findings suggest that short and long GRBs might originate from different progenitors (Mészáros 2006; Berger 2013).

Observationally, the most important difference between short and long GRBs is their T_{90} duration. A first attempt to compare the spectral properties of short and long GRBs detected by *CGRO*/BATSE showed that (i) the difference in hardness could be due to a harder low energy spectral index of short GRBs rather than a harder peak energy and (ii) that the spectra of SGRBs and the first 1–2 s of LGRBs appear similar (Ghirlanda et al. 2004). These results suggested that the engine might be similar in the two classes, but the ac-

* E-mail: giorgio.calderone@gmail.com

tivity would last longer in the case of LGRBs (Guiriec et al. 2010). Also, Nakar & Piran (2002) found that the ratio of the shortest pulse duration to the total burst duration for both short and the first 1–2 s of long GRBs were comparable.

With the advent of the Gamma Burst Monitor (GBM) on board *Fermi*, it became possible to compare the spectral properties of large samples of short and long GRBs and to compare them with those detected by *CGRO*/BATSE. Nava et al. (2011a) showed that long and short GRBs occupy different regions in the observer frame hardness (defined by the peak of the νF_ν spectrum) versus fluence, with SGRBs having smaller fluences than long events. This also suggested that the possible selection of fluence limited samples for the comparison of SGRBs and LGRBs could introduce biases.

The availability of redshift estimates for long GRBs allowed one to estimate their rest frame (intrinsic) spectral properties, and to highlight a few correlations among them (see Ghirlanda et al. 2006 for a review). Amati et al. (2002) found that the rest frame νL_ν peak energy (E_p) is correlated with the total energy emitted in the 1 keV–10 MeV energy range (under the hypothesis of isotropic emission, E_{iso}), with a slope of ~ 0.5 . Yonetoku et al. (2004) found a correlation between E_p and the isotropic peak luminosity evaluated at the flux peak over an interval of 1 s ($L_{p,\text{iso}}$), with a slope of ~ 0.4 . The latter correlation is valid also when considering the time resolved spectral quantities $E_p(t)$ and $L_{\text{iso}}(t)$ of a single burst, i.e. the evolutionary tracks of GRB spectra in the E_p – L_{iso} plane align with the Yonetoku relation (Firmani et al. 2009; Ghirlanda et al. 2010; Frontera et al. 2012).

With the fast slewing *Swift* satellite (Gehrels et al. 2004) it became possible to localize the X–ray afterglows of short GRBs, and estimate their redshifts by means of the associated host galaxies (Gehrels et al. 2005). The comparison of intrinsic spectral properties of short and long GRBs have shown that short GRBs are consistent with the Yonetoku relation, but are significant outliers of the Amati relation (Amati 2006, 2008; Ghirlanda et al. 2009; D’Avanzo et al. 2014). However, by analyzing a sample of 7 short GRBs, Zhang et al. (2012) suggest that short GRBs might follow a parallel Amati relation at lower values of E_{iso} . Moreover, the SGRBs follow the same three parameter correlation ($E_{X,\text{iso}}-E_{\gamma,\text{iso}}-E_p$) valid for long GRBs (Bernardini et al. 2012; Margutti et al. 2013). The isotropic luminosities are similar in both short and long GRBs, but the former are less energetic than the latter by a factor similar to the ratio of their durations. When considering the time averaged spectra, short GRBs have harder low–energy spectral index, but this difference vanishes when comparing the SGRBs with only the first 1–2 s of long GRBs (Ghirlanda et al. 2009).

Also the time resolved spectroscopy has shown that the observed peak energy tracks the flux evolution in both short and long GRBs (Guiriec et al. 2010; Ghirlanda et al. 2011a), suggesting a common physical mechanism linking these quantities. The existence of a time resolved correlation between $E_p(t)$ and $L_{\text{iso}}(t)$ was also shown to hold in short GRBs (Ghirlanda et al. 2011a). This is the most compelling evidence that the $E_p(t)$ – $L_{\text{iso}}(t)$ correlation holding in long and short GRBs (with similar slope and normalization) hints to a common origin which could be related to the emission mechanism (Ghirlanda et al. 2011a) and that the corresponding Yonetoku correlation (holding between time integrated properties) cannot be subject to strong selection ef-

fects. An interesting hypothesis discussed in Ghirlanda et al. (2009, 2011a); Guiriec et al. (2013) is that both short and long GRBs may share a common emission process, and that the observed differences may be ascribed to the different engine lifetime of their progenitors.

Yet, the comparison of short and long GRBs in search for possible similarities or differences should account for their possible different redshift distributions. While several LGRBs have their redshift measured, the population of short bursts still suffers from a lack of redshift measures. However, recent collection of small, well defined, samples of SGRBs with measured redshifts (e.g. D’Avanzo et al. 2014) allowed us to compare the energetic properties of short and long events in their rest frame.

The aim of this work is to further explore the similarities between short and long GRBs by comparing their intrinsic (i.e. rest frame) spectral properties estimated on the same rest frame time scales. The average $T_{90}/(1+z)$ duration of the short GRBs with reliable (spectroscopic) redshifts and without X–ray extended emission in the D’Avanzo et al. (2014) sample is 0.3 s (10 bursts). This will be our reference time scale to perform spectral analysis of the first part of long GRBs, and compare the results with those of short GRBs.

Throughout the paper, we assume a Λ CDM cosmology with $H_0 = 71 \text{ km s}^{-1} \text{ Mpc}^{-1}$, $\Omega_m = 0.27$, $\Omega_\Lambda = 0.73$.

2 THE SAMPLE

Since we aim to study the prompt emission spectral properties and energetic/luminosity of GRBs, we need a broad energy coverage in order to determine where the peak energy is. While *Swift*/BAT has a limited energy range (15–150keV) which is not suited for GRB prompt emission spectral characterization, the GBM instrument on board *Fermi* covers almost 2 orders of magnitude in energy with the NaI detectors (8keV–1MeV) and can extend this energy range to a few tens of MeV with the inclusion of the data of the BGO detectors. Hence we selected all GRBs observed by *Fermi*/GBM up to December 2013 with a redshift estimate. This amounts to 64 long and 7 short GRBs.

Among the long ones we discarded: 2 GRBs with missing response matrix files; 2 GRBs observed with a non–standard Low Level Threshold¹; 3 GRBs whose first part was missed by the GBM; 12 GRBs for which we could not constrain either the low energy spectral index or the peak energy (§3). The final LGRB sample comprises 45 long bursts.

Fermi/GBM observed 7 short GRBs with known redshift. To this sample we added the SGRB flux limited sample of 12 sources with redshift discussed in D’Avanzo et al. (2014, hereafter D14 sample), but discarded: GRB 080905A since its redshift is likely not accurate, GRB 090426 and GRB 100816A since their classification as short GRB is debated. Four GRBs in the D14 sample were also in the GBM sample: for these bursts we considered the results reported in D14. The final SGRB sample comprises 3 GRB observed with *Fermi*/GBM and 9 from D14.

The short GRB sample, although relatively small, stems

¹ http://fermi.gsfc.nasa.gov/ssc/data/access/gbm/llt_settings.html

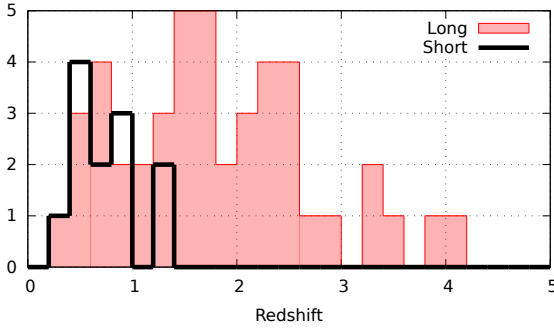


Figure 1. Redshift distribution for both the SGRB (12) and LGRB (45) bursts (references for redshift estimates are given in Tab.A1).

from a flux limited sample of short GRB with a redshift completeness of $\sim 70\%$ (D’Avanzo et al. 2014). We dropped three burst from this sample, hence the redshift completeness drops to $\sim 60\%$, but we added three more bursts detected by *Fermi*/GBM. The distributions of low-energy spectral index in both our short sample and the corresponding one² in the Gruber et al. (2014) catalog are actually indistinguishable (K–S test probability: 0.47). Since the spectral index is a redshift independent property we assume that our short GRB sample is a reasonably good representation of the parent distribution of short GRBs observable with currently available detectors.

The total (LGRB+SGRB) comprises 57 bursts (Tab.A1). Fig. 1 shows the redshift distribution for both the SGRB and LGRB samples (references for redshift estimates are given in Tab.A1).

3 DATA ANALYSIS

Our spectral analysis aims at estimating the intrinsic peak energy (E_p), isotropic equivalent luminosity (L_{iso}) and emitted energy (E_{iso}) for the GRBs in our sample. For the 3 short GRBs observed by *Fermi*/GBM we performed a spectral analysis on the entire duration of the burst (*short* analysis). For the remaining 9 SGRB we considered the spectral properties relative to the time integrated emission reported in the D14 paper (*short D14*). For the 45 long GRBs we perform two different spectral analysis: one for the first 0.3 s in the rest frame (corresponding to $0.3 \times (1+z)$ s in the observer frame, *first* analysis) and one for the whole duration of the burst (*whole* analysis). All E_{iso} and L_{iso} quantities are evaluated in the (rest frame) energy range 1 keV–10 MeV.

All data analysis has been carried according to the procedure outlined below.

3.1 Detectors, energy selection and background fitting

For each GRB we selected the most illuminated NaI detector(s), and the corresponding BGO one. The BGO detector is always included, even if there is no significant detection

² Bursts with $T_{90} < 2$ s and a either a Band or cutoff power law best fitting model in the Gruber et al. (2014) catalog: 70 GRB.

above background. The energy selection is in the range 8–800 keV for NaI detectors, and 200 keV–35 MeV for BGO ones. Systematic residuals at ~ 33 keV of the NaI detectors³ are neglected.

For each channel of all detectors we perform a polynomial fit (up to the third order) to the observed background count rate in the CSPEC files,⁴ on a time interval before and after the burst longer than the burst duration (typically $\gtrsim 100$ s). The length of the background time intervals is progressively increased until the uncertainties on the expected background counts during the burst becomes smaller than their intrinsic statistical fluctuations. This approach provides an objective way to select the background time intervals. We also checked that the background fit provide an adequate fit for all energy channels by means of χ^2 goodness-of-fit test. For long bursts, we used exactly the same background model for both the *first* and *whole* analysis.

The detectors used and the background time selections for each burst are shown in Tab. A1.

3.2 Time selection

For the GRB spectral analysis we used the TTE data files⁵ to select the counts in the appropriate time intervals: either the first 0.3 seconds (rest frame) for the *first* analysis, or the whole burst duration for both the *short* and *whole* analysis.

For the *short* and *whole* analysis of GRBs present in both our sample and the Gruber et al. (2014) catalog we consider their time selection. This choice allows us to compare our results with those of Gruber et al. (2014), as discussed in §B. For the other bursts the time selection was performed by a visual inspection of the count rate light curves.

For the *first* analysis we searched for the first occurrence of a 0.3 s long (rest frame) time bin in which the counts in all NaI detectors were significantly (at 3σ level) above the expected background. The search has been performed with a 0.2 s resolution starting at 10 s before the trigger time.

The time selections for each burst are shown in Tab. A2.

3.3 Spectral fitting

The GRB spectral models used for spectral analysis are a modified version⁶ of either the cutoff power law or the Band model (Band et al. 1993), in which the free parameters are:

- **log_Ep**: the logarithm of the νF_ν peak energy in keV;
- **alpha**: the photon spectral index for energies smaller than the peak energy;
- **beta** (only for the Band model): the photon spectral index for energies greater than the peak energy;

³ http://fermi.gsfc.nasa.gov/ssc/data/analysis/GBM_caveats.html

⁴ Time binned count spectra with time resolution of 1.024 s from the burst trigger time T_0 to T_0+600 s, and time resolution of 4.096 s for a few thousands seconds before and after the burst.

⁵ The list of all recorded counts with time and channel tags (Time Tagged Events). Data are available from $\sim T_0 - 25$ s to $\sim T_0 + 300$ s.

⁶ The XSPEC implementation of this spectral model is available http://www.giorgiocalderone.url.ph/xspec_ggrb.tar.gz.

- `log_F`: the logarithm of the integrated flux in the rest frame energy range 1 keV–10 MeV.

The spectral indices are bounded to be `alpha` > -2 and $-6 < \text{beta} < -1.7$. For the *whole* spectral analysis we also included detectors effective area correction as free parameters, bounded in the range 0.5–2. Whenever the resulting area corrections are not constrained we set all calibration factors to one. The `log_F` parameter is used to estimate the intrinsic isotropic luminosity $L_{\text{iso}} = 4\pi D_L^2 \times F$, without the need to propagate the uncertainties on the other parameters. Finally, isotropic emitted energy is estimated as $E_{\text{iso}} = L_{\text{iso}} \Delta T_{\text{rest}}$, where $\Delta T_{\text{rest}} \times (1+z)$ is the spectrum integration time.

The spectral model is folded with the detector response matrix, summed with the background counts expected in the same time interval, and compared to the observed counts by means of the Cash statistic (Cash 1979) with Castor normalization (C-STAT). The model fitting is performed with `xspec` ver. 12.8.1g (Arnaud 1996) by minimizing the C-STAT value. We always used the detector maximum energy resolution, i.e. we did not rebin the channels.

The choice of the spectral model (cutoff power law or Band) is performed according to the following criterion: for each burst we started with the Band model with both spectral indices free to vary in the minimization process. If the `beta` parameter uncertainty is larger than a nominal threshold of 0.5, but still significantly lower than the `alpha` parameter, we fixed `beta` to its typical value, namely -2.3 (Band et al. 1993; Ghirlanda et al. 2002), and repeat the fit. If `beta` hits the lower limit (-6) we use the cutoff power law model instead of the Band model. If `beta` is > -2 and `alpha` $>$ `beta` we consider the resulting E_p and L_{iso} as lower limits. The true location of the $\nu F\nu$ peak likely lies on the extrapolation of the spectrum actually constrained by the data. By assuming `alpha` $= -1$ (the typical value for this parameter, Nava et al. 2011b), this extrapolation lies on a line of slope 1 in the E_p – L_{iso} plane.

In 12 cases we could not detect a curvature in the spectrum, i.e. we could not constrain either the `alpha` or the `log_Ep` parameters. These bursts were discarded from our sample (§2).

The parameter uncertainties (quoted at 1σ) for the *whole* analysis are estimated with the usual $\Delta\chi^2$ method (Avni 1976; Cash 1976). For the *short* and *first* analysis we adopted a different approach since the counts in the high-energy channels of the detectors are often very low. In these cases we start by performing a fit in the usual way, and use the best fit parameter estimates to simulate several data sets for each detector (using the `fakeit` command). Then we run the fitting process on the mock data sets, and consider the distribution of the resulting best fit parameters. The final uncertainties are estimated as the central interval containing 68.3% of the best fit values. The simulation iterates until the lower and upper limits of the confidence interval change by less than 5%. Typically 400–600 simulations are required to satisfy the convergence criterion. This Monte Carlo method is described in detail in Press et al. (2007, their Sect. 15.6.1).

In §B we compare the results of our *whole* analysis to those of Gruber et al. (2014), for the bursts present in both samples, and show that the two methods produce very sim-

ilar results. However, our method ensures a homogeneous approach in all our spectral analysis: we established an objective criterion to select the background time intervals, and used exactly the same background model in both the *first* and *whole* analysis. The use of logarithmic quantities in our spectral model results in simpler and more symmetric parameter uncertainties, with respect to their linear counterparts (e.g. Cabrera et al. 2007). Also, the use of the integrated flux as model parameter, instead of the flux at a given energy, allows us to directly evaluate the uncertainties on L_{iso} , avoiding the necessity to estimate the parameter covariance matrix for error propagation. Finally, the use of Monte Carlo simulations in the *short* and *first* analysis provide reliable parameter uncertainties even in the low count regime, when the assumption that the C-STAT value is drawn from a χ^2 distribution is not reliable.

3.4 Results

The results of spectral analysis, as well as the spectral quantities reported in D14 for the short GRB sample, are shown in Tab. A2. The relevant quantities for the *short*, *first* and *whole* sub samples are shown in Fig. 2. The lower limits for E_p and E_{iso} (2 in the *short*, 4 in the *first* and 3 in the *whole* analysis, respectively) are not accounted for in the histograms.

Fig. 3 (left panel) shows the ratio of *first* to *whole* peak energy vs. the same ratio of E_{iso} . The blue dashed lines are the median values of both ratios. The right panel shows the $E_{\text{iso,whole}}/E_{\text{iso,first}}$ ratio vs. $\Delta T_{\text{whole}}/\Delta T_{\text{first}}$. The blue dashed line is the 1:1 line. The numbers beside the symbols are the GRB identifiers shown in Table A1 and A2.

Finally, in Fig. 4 and 5 we show the location of all bursts in the E_p – E_{iso} and E_p – L_{iso} planes respectively. The lower limits are shown with arrows of slope 1, as discussed in §3.3.

3.5 Notes on individual bursts

- GRB 091024 (Gruber et al. 2011; Nappo et al. 2014): the GBM data are separated in two burst intervals, hence this GRB appear twice in Tab. A1 (ID 23). The first interval is actually a precursor and it is analysed according to the *first* prescription. The second interval comprises a second precursor and the main event. The *first* analysis at the beginning of the main event did not provide reliable constraints on the peak energy, hence we consider only the *whole* analysis.

- GRB 110213: for this burst the *first* analysis did not provide reliable constraints on the peak energy because the signal is significantly background dominated, hence we consider only the *whole* analysis.

- GRB 120711A and GRB 120716A show a precursor in their light curve. For these bursts we analysed the precursor spectra according to the *first* analysis.

- GRB 130427A: the GBM data are unreliable after ~ 4 seconds from the trigger since the large amount of recorded events, due to the exceptional brightness of this burst, saturated the available bandwidth (Preece et al. 2014). Hence we consider only the *first* analysis for this burst.

By taking into account these notes the final subsamples

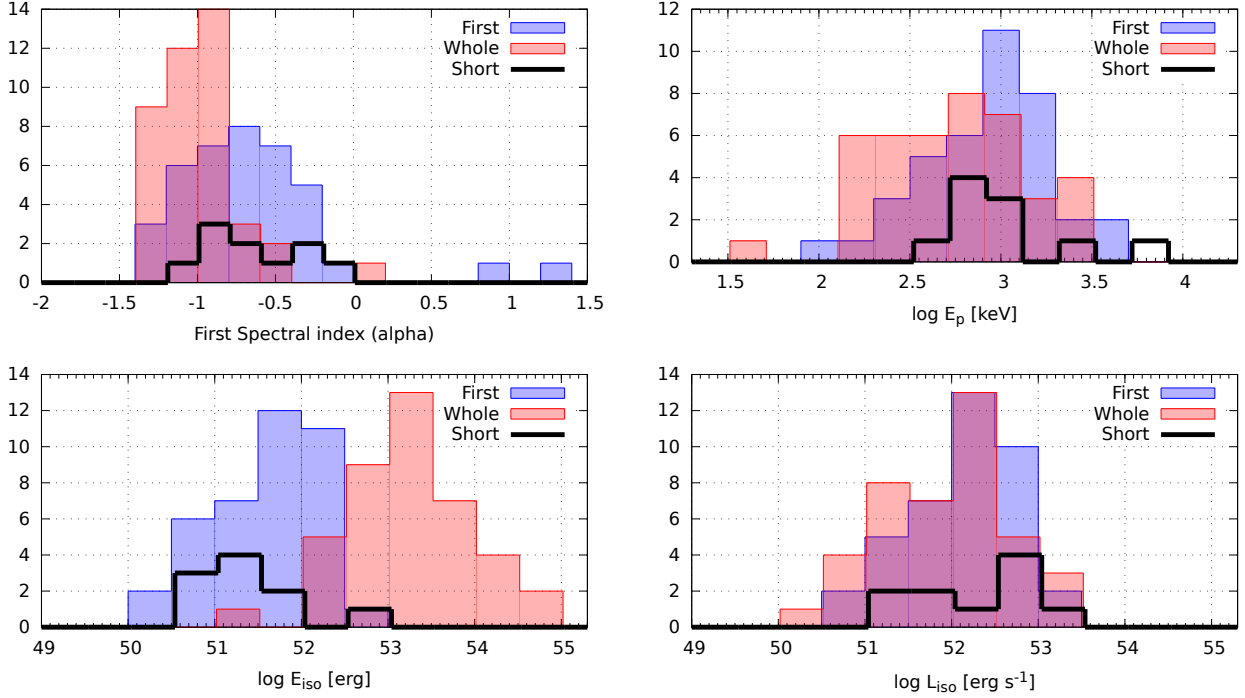


Figure 2. Histograms of relevant results of the spectral analysis. Upper panels: the low energy spectral index α (left); intrinsic νL_ν peak energy E_p (right). Lower panels: isotropic equivalent, emitted energy E_{iso} (left) and luminosity L_{iso} (right), integrated in the 1 keV–10 MeV energy range (rest frame). The lower limits for E_p and E_{iso} and the analysis on precursors are not accounted for in the histograms.

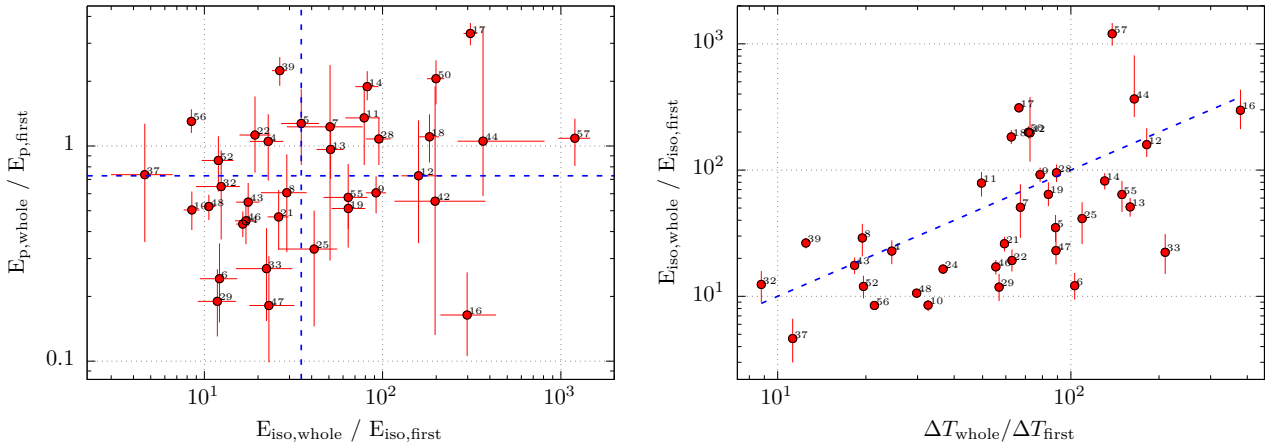


Figure 3. Left panel: ratio of *whole* to *first* peak energy vs. the same ratio for E_{iso} . The blue dashed lines are the median values of both ratios. Right panel: the $E_{\text{iso,whole}}/E_{\text{iso,first}}$ ratio vs. $\Delta T_{\text{whole}}/\Delta T_{\text{first}}$. The blue dashed line is the 1:1 line. The numbers beside the symbols are the GRB identifiers shown in Table A1 and A2.

comprises:

Short : 12 bursts, with 2 lower limits
First : 43 bursts, with 4 lower limits
Whole : 44 bursts, with 3 lower limits

3.6 E_p – E_{iso} and E_p – L_{iso} correlations

We use the results of the spectral analysis to test the spectral–energy correlations in the E_p – E_{iso} and E_p – L_{iso} planes. The former is the Amati relation, while the second is only similar to the Yonetoku relation, since we use the L_{iso} values estimated on the time averaged spectra, rather than the peak isotropic luminosity $L_{p,\text{iso}}$ (Yonetoku et al. 2004).

We estimate the Spearman rank correlation coefficients

and the associated chance probability for the *short*, *first* and *whole* results. Also, we estimate the best fit correlations by applying the unweighted bisector method (Isobe et al. 1990). Lower limits and precursor data are not considered in this analysis. The histograms of the residuals from the best fit line, once projected on a scale perpendicular to the line itself, are fitted with a Gaussian function in order to estimate the scatter (σ_{sc}) from the best fit. Results are shown in Tab.1.

In Fig. 4 we show the best fit correlations (solid lines) on the E_p - E_{iso} plane for the *short* (purple), *first* (blue) and *whole* (red) results, as well as the histograms of residuals (inset plots). For comparison we also plot the corresponding relations from the total sample of Nava et al. (2012) (black dashed line) and from both the short and long GRB sample of Zhang et al. (2012) (double dot-dashed lines). In Fig. 5 we show the corresponding results in the E_p - L_{iso} plane. For comparison we show the E_p - $L_{p,iso}$ relations from the total sample of Nava et al. (2012) (black dashed line) and from the combined short and long GRB sample of Zhang et al. (2012) (double dot-dashed lines).

4 DISCUSSION AND CONCLUSIONS

We performed the spectral analysis of a sample long GRBs observed by *Fermi*/GBM with a redshift estimate, using time integration equal to 0.3 s rest frame (*first* analysis) and to the whole burst duration (*whole* analysis). Besides, we considered a sample of short GRBs (*short* analysis), both by performing spectral analysis of *Fermi*/GBM data and by reporting data from D’Avanzo et al. (2014, D14 sample). Our aim is to compare the results of the *first* analysis to those of the *short* and *whole* analysis. The comparison of the relevant quantities are shown in Fig. 2. Tab. 2 shows the probability that the distributions of the quantities shown in Fig. 2 are drawn from the same parent population.

The distributions of both E_p and L_{iso} are similar for the *short*, *first* and *whole* results. The distributions of low energy spectral index (α) for the *short* and *first* results are very similar, but the distribution for the *whole* results is significantly different (K-S test probabilities 5.3×10^{-5} and 8.9×10^{-4} , when compared to *first* and *short* results respectively), with the latter showing lower values of α . Also, the distribution of E_{iso} of the *whole* results is significantly different from the *first* and *short* results (K-S test probability: 4.1×10^{-13} and 2.1×10^{-6} , when compared to *first* and *short* results respectively), with the *whole* results lying a factor of a few tens above the others.

The peak energy E_p of long GRBs, going from the first 0.3 s (rest frame) to the whole burst duration, evolves either to lower or higher energies, hence we do not find strong evidence for hard-to-soft evolution of the peak energy. The logarithmic median value of the *whole* to *first* E_p ratio is ~ 0.7 (Fig. 3, left panel). The total emitted energy E_{iso} increases by a factor 5–10³, with a logarithmic median of ~ 35 . It is not clear what drives the evolution of E_p towards either lower or higher energies, since the $E_{p,whole}/E_{p,first}$ ratio does not show a clear correlation with any other quantity. The main driver for the E_{iso} evolution is the total burst duration $\Delta T_{whole,rest}$, i.e. longer burst likely evolve towards higher E_{iso} (Fig. 3, right panel).

As discussed in §2 the short GRB sample, although rel-

atively small when compared to the long sample, is a reasonably good representation of the parent distribution of short GRBs observable with currently available detectors. Moreover, the short GRB sample is large enough to provide evidence for significant different distributions of α and E_{iso} when compared to the *whole* sample. Hence the K-S tests to compare the spectral properties of the *short* and *first* samples are reliable, and the corresponding distributions are actually indistinguishable, i.e. we are unable to distinguish a short GRB from the first 0.3 seconds of a long one with currently available detectors. Clearly, as new redshift estimates for SGRB become available, our results may need to be reconsidered.

The plot of the E_p - E_{iso} plane is shown in Fig. 4. There is a clear correlation between E_p and E_{iso} for the *whole* results, with a chance probability of obtaining a higher value of the Spearman’s rank correlation of $\sim 10^{-7}$ (Tab. 1). In the E_p - E_{iso} plane this is the well known Amati relation (Amati et al. 2002). The correlation slope and scatter (0.57 ± 0.06 and 0.25) are very similar to the ones found in Nava et al. (2012) for their total sample (0.55 ± 0.02 , 0.23), and in Zhang et al. (2012) for their long GRB sample (0.51 ± 0.03). For the *first* results we found a new E_p - E_{iso} relation with a probability $\sim 10^{-3}$ of being spurious. The best fit *whole* relation lies at 3–4 σ_{sc} away from the *first* relation, hence the *first* and *whole* populations are well separated in the E_p - E_{iso} plane. The *short* GRBs alone do not provide a strong statistical evidence for the existence of such a correlation ($P_{chance} = 0.02$). However, all *short* results lie within $2\sigma_{sc}$ from the best fit relation for the *first* results. Moreover, the best fit *short* correlation, if it actually exists, lies very close to the *first* one, and significantly away from the *whole* one. Therefore, the *short* and *first* results are actually indistinguishable in the E_p - E_{iso} plane. The lower limits for E_p and E_{iso} were not considered in the correlation analysis. However, the true values of E_p and E_{iso} of the *short* and *first* population are not supposed to lie closer to the *whole* correlation than their lower limits, as shown by the arrows in Fig. 4. Hence our conclusions can not be hampered by the presence of lower limits. GRB precursors, when present, also lie in the *short*-*first* region.

In the E_p - L_{iso} (Fig. 5) similar considerations apply: there is a strong correlation for the *whole* results, a marginally significant correlation for the *first* results⁷, and a weak correlation for the *short* results. However, in the E_p - L_{iso} plane all correlations overlap and are very similar. Note that these correlations are not equivalent to the Yonetoku relation, since we used the L_{iso} values estimated on the time averaged spectra, rather than the peak isotropic luminosity $L_{p,iso}$ (Yonetoku et al. 2004). Hence, we do not expect to find the same results found in literature. In particular we expect our results to lie at lower L_{iso} since the peak luminosity is by definition the highest luminosity for each burst. Indeed the Yonetoku relation found in Nava et al. (2012) for their total sample, and by Zhang et al. (2012) for their combined short and long sample, lie on the right of our best fit correlation. Nevertheless, our analysis shows that the E_p -

⁷ The correlation analysis for the *first* results are the same in both the E_p - E_{iso} and E_p - L_{iso} planes, since the rest frame time interval is the same for all GRBs: 0.3 seconds.

Table 1. Results of the statistical analysis of the E_p - E_{iso} and E_p - L_{iso} correlations for the *short*, *first* and *whole* results. A , B and γ are the correlation parameters, while ρ_s and P_{chance} are the Spearman's rank correlation coefficient and the associated chance probability. Results from precursors data are not considered.

Correlation	Results	No. GRBs	A	B	γ	σ_{sc}	ρ_s	P_{chance}
$\log \frac{E_p}{\text{keV}} = \gamma(\log \frac{E_{\text{iso}}}{\text{erg}} - A) + B$	<i>short</i>	10	51.45	2.99	0.59 ± 0.07	0.15	0.71	0.02
	<i>first</i>	39	51.62	2.92	0.65 ± 0.07	0.29	0.50	1×10^{-3}
	<i>whole</i>	41	53.21	2.73	0.57 ± 0.06	0.25	0.73	5×10^{-8}
$\log \frac{E_p}{\text{keV}} = \gamma(\log \frac{L_{\text{iso}}}{\text{erg s}^{-1}} - A) + B$	<i>short</i>	10	52.28	2.99	0.63 ± 0.11	0.30	0.50	0.14
	<i>first</i>	39	52.15	2.92	0.65 ± 0.07	0.29	0.50	1×10^{-3}
	<i>whole</i>	41	51.92	2.73	0.58 ± 0.07	0.29	0.7	4×10^{-7}

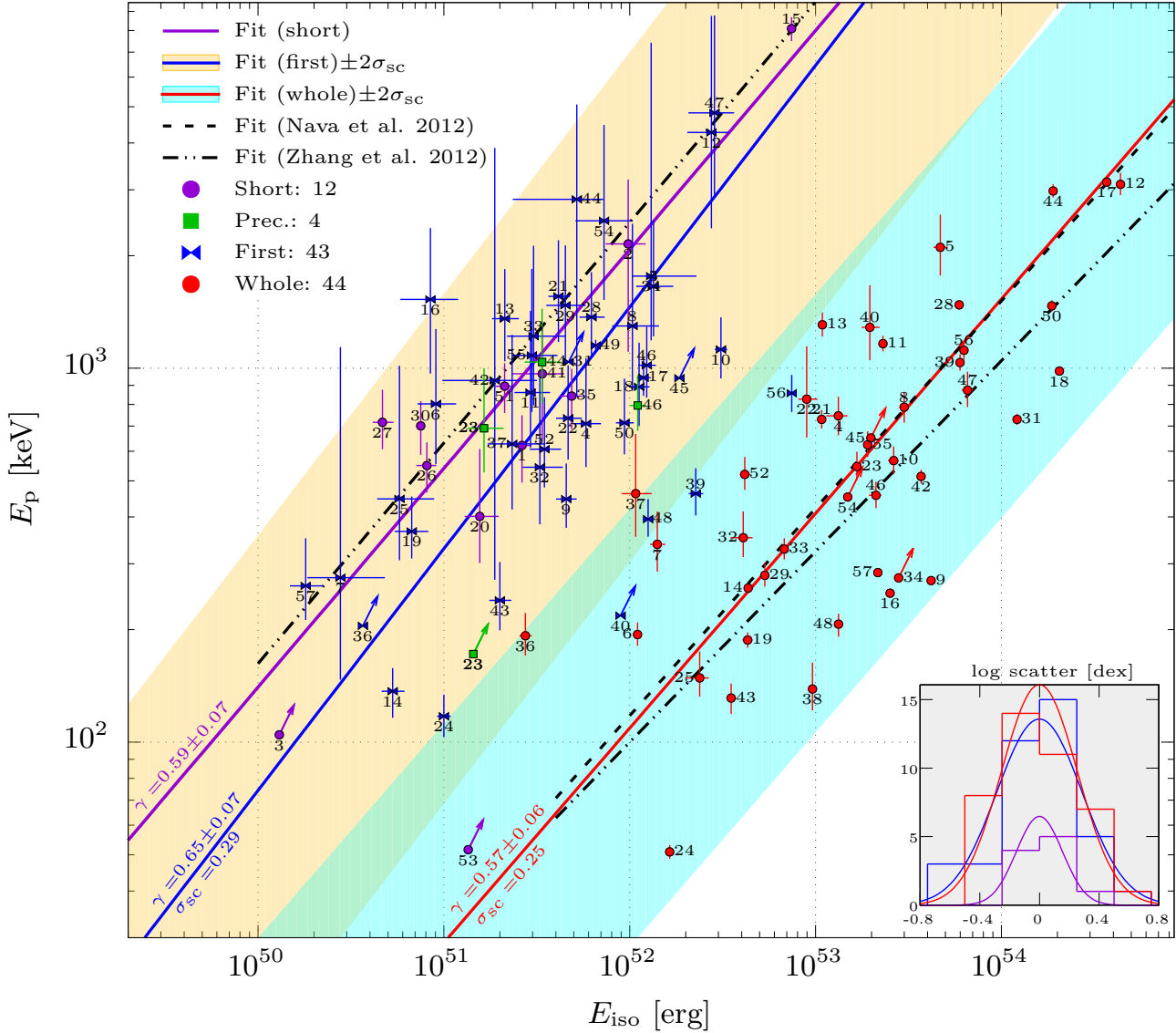


Figure 4. Rest frame E_p - E_{iso} plane for all GRBs considered in this work. The *short*, *first* and *whole* analysis results are shown with purple, blue and red symbols respectively, while the best fit correlations are shown with solid lines of the corresponding colors. The numerical values of the slope and the scatter of the correlations are shown near the edges of the plots. The inset plots show the histogram of the residuals from the best fit correlations. The *first* analysis on precursors data are shown with green symbols. The shaded areas are the $2\sigma_{\text{sc}}$ of the correlations of the *first* (orange) and *whole* (cyan) results. Also shown are the E_p - E_{iso} relations from the total sample of Nava et al. (2012) (black dashed line) and from both the short and long GRB sample of Zhang et al. (2012) (double dot-dashed lines) for comparison.

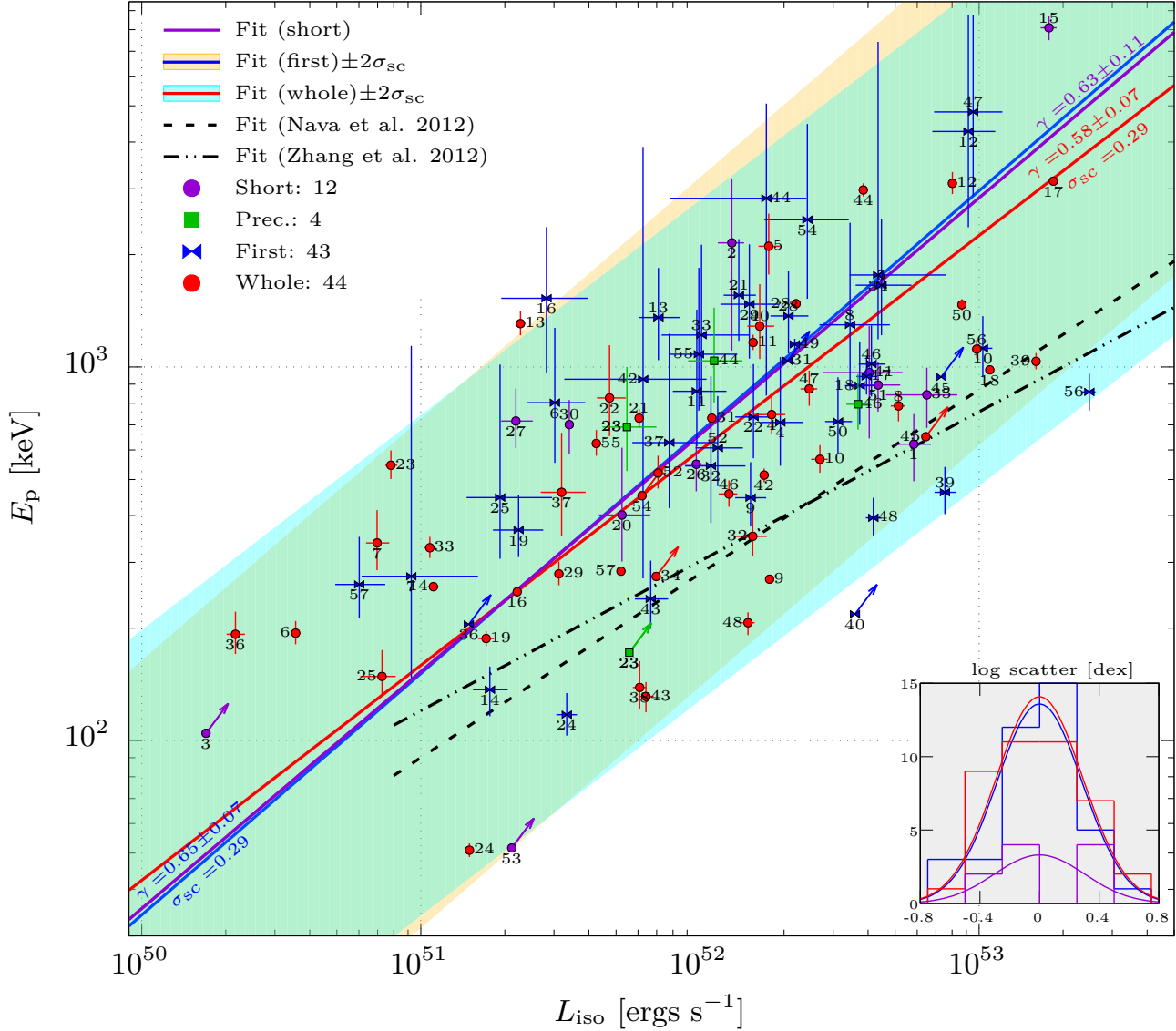


Figure 5. Rest frame E_p - L_{iso} plane for all GRBs considered in this work with the same colors and symbols used in Fig. 4. Also shown are the E_p - $L_{p,\text{iso}}$ relations from the total sample of Nava et al. (2012) (black dashed line) and from the combined short and long GRB sample of Zhang et al. (2012) (double dot-dashed lines).

Table 2. Results of Kolmogorov–Smirnov tests: column 2 and 3 show the probability that the distributions of the quantity shown in column 1 for the *short*, *first* and *whole* results are drawn from the same parent population.

Quantity	<i>Short</i> vs. <i>First</i>	<i>Whole</i> vs. <i>First</i>	<i>Whole</i> vs. <i>Short</i>
alpha	0.83	5.3×10^{-5}	8.9×10^{-4}
$\log E_p$	0.71	0.11	0.10
$\log E_{\text{iso}}$	0.43	4.1×10^{-13}	2.1×10^{-6}
$\log L_{\text{iso}}$	0.54	0.19	0.29

L_{iso} relation turns out to be very similar for the *first* and *short* results (under the assumption that the latter actually exists). Hence, these correlations are possibly the manifestation of the same physical process acting in all GRBs, and even in small temporal intervals within a single GRB.

It has been debated if the E_p -Eiso and E_p -Liso correla-

tion are affected by selection effects (Band & Preece 2005; Nakar & Piran 2005; Butler et al. 2007, 2009; Shahmoradi & Nemiroff 2011; Kocevski 2012). The possible existence of similar correlation within individual GRBs, i.e. between the peak energy and the luminosity as a function of time in a single GRB (Firmani et al. 2009; Ghirlanda et al. 2010,

2011a,b; Frontera et al. 2012) seems to point to a physical origin of these correlations. Similarly the use of a flux limited complete sample of long GRBs seems to support the idea that instrumental selection effects are not shaping these correlations (Nava et al. 2012; Ghirlanda et al. 2012). Hence these correlations are likely the manifestation of fundamental GRB properties. Since our correlations for the *whole* analysis (Tab. 1) are very similar to those found in literature we do not expect our long sample to be strongly biased by selection effects. As a consequence, also the *first* correlation is not biased, since the sample is the same. The *short* analysis, on the other hand, has been performed on a flux limited short GRB sample with a redshift completeness of $\sim 60\%$, hence we do not expect the selection effects (beyond the limiting flux threshold) to play a dominant role.

The 0.3 s (rest frame) time scale chosen for the *first* analysis has a clear interpretation: it is the representative duration of the short GRBs in the D14 catalog. Since the main driver for the E_{iso} evolution is the integration time (Fig. 3, right panel), a longer timescale would result in higher values of $E_{\text{iso,first}}$. Hence, in order to obtain significantly higher (or lower) values of E_{iso} , we should overcome the intrinsic scatter of the correlations, namely 0.25–0.3 dex (a factor ~ 2 , i.e. $\Delta T_{\text{first}} \lesssim 0.15$ s or $\Delta T_{\text{first}} \gtrsim 0.6$ s).

In summary, we found that the intrinsic spectral properties (peak energy and luminosity) of both the short GRBs and the first 0.3 s (rest frame) of long ones are actually indistinguishable. Hence if the central engine of a long GRB would stop working after ~ 0.3 s, we would have no means to distinguish it from a genuine short GRB. Clearly, short and long GRBs remains two distinct phenomena, each one with its own duration. In particular short GRBs lasts longer or shorter than 0.3 s. Likewise, we do not expect the short-like phase at the beginning of long GRBs to always lasts 0.3 s. Our findings are in agreement with those in Ghirlanda et al. (2009), which found no differences in the (observed) spectral properties of short GRBs and the first 1–2 s of long GRBs. We extended this work by comparing the intrinsic (rest frame) properties rather than the observed ones.

Moreover, we found that the spectral quantities in the first 0.3 s of long GRBs define new E_p – E_{iso} and E_p – L_{iso} correlations. These correlations are possibly the manifestation of an underlying physical process common to all GRBs, despite the possibly different progenitors of short and long GRBs, and the great variety of energetics and spectral properties involved.

ACKNOWLEDGMENTS

We gratefully acknowledge the Referee for the useful comments and suggestions which greatly improved the paper. The research activity of A. Melandri, M.G. Bernardini and P. D’Avanzo is supported by ASI grant INAF I/004/11/1. G. Calderone was supported by PRIN INAF 2011 (1.05.01.09.15).

REFERENCES

- Amati L., 2006, MNRAS, 372, 233
 Amati L., 2008, in Bianco C. L., Xue S.-S., eds, Relativistic Astrophysics Vol. 966 of American Institute of Physics Conference Series, Spectrum-Energy Correlations and Swift GRBs. pp 3–6
 Amati L., et al., 2002, A&A, 390, 81
 Arnaud K. A., 1996, in Jacoby G. H., Barnes J., eds, Astronomical Data Analysis Software and Systems V Vol. 101 of Astronomical Society of the Pacific Conference Series, XSPEC: The First Ten Years. p. 17
 Avni Y., 1976, ApJ, 210, 642
 Band D., et al., 1993, ApJ, 413, 281
 Band D. L., Preece R. D., 2005, ApJ, 627, 319
 Berger E., 2013, arXiv:1311.2603
 Berger E., M. Rauch M., 2008, GCN 8542
 Bernardini M. G., Margutti R., Zaninoni E., Chincarini G., 2012, MNRAS, 425, 1199
 Bromberg O., Nakar E., Piran T., Sari R., 2013, ApJ, 764, 179
 Butler N. R., Kocevski D., Bloom J. S., 2009, ApJ, 694, 76
 Butler N. R., Kocevski D., Bloom J. S., Curtis J. L., 2007, ApJ, 671, 656
 Cabrera J. I., Firmani C., Avila-Reese V., Ghirlanda G., Ghisellini G., Nava L., 2007, MNRAS, 382, 342
 Cash W., 1976, A&A, 52, 307
 Cash W., 1979, ApJ, 228, 939
 Cenko S. B., et al., 2009a, GCN 9053
 Cenko S. B., et al., 2009b, GCN 9518
 Chornock R., Berger E., Fox D., 2011, GCN 11538
 Chornock R., et al., 2009a, GCN 9028
 Chornock R., et al., 2009b, GCN 9243
 Chornock R., Lunnan R., Berger E., 2013, GCN 15307
 Cucchiara A., et al., 2008, GCN 8713
 Cucchiara A., et al., 2009a, GCN 9873
 Cucchiara A., et al., 2009b, GCN 10031
 Cucchiara A., et al., 2009c, GCN 10065
 Cucchiara A., et al., 2009d, GCN 10202
 Cucchiara A., et al., 2010, GCN 10606
 Cucchiara A., et al., 2012, GCN 12865
 Cucchiara A., et al., 2013, GCN 14687
 D’Avanzo P., et al., 2011, GCN 12284
 D’Avanzo P., Salvaterra R., Bernardini M. G., Nava L., Campana S., Covino S., D’Elia V., Ghirlanda G., Ghisellini G., Melandri A., Sbarufatti B., Vergani S. D., Tagliaferri G., 2014, arXiv:1405.5131
 de Ugarte Postigo A., et al., 2009, GCN 8766
 de Ugarte Postigo A., et al., 2013, GCN 15470
 D’Elia V., et al., 2012, GCN 13494
 Firmani C., Cabrera J. I., Avila-Reese V., Ghisellini G., Ghirlanda G., Nava L., Bosnjak Z., 2009, MNRAS, 393, 1209
 Flores H., et al., 2010, GCN 11317
 Flores H., et al., 2013, GCN 14491
 Frontera F., Amati L., Guidorzi C., Landi R., in’t Zand J., 2012, ApJ, 754, 138
 Fynbo J. P. U., et al., 2008, GCN 8254
 Fynbo J. P. U., et al., 2009, GCN 9947
 Gehrels N., et al., 2004, ApJ, 611, 1005
 Gehrels N., et al., 2005, Nature, 437, 851
 Gehrels N., et al., 2008, ApJ, 689, 1161
 Ghirlanda G., Celotti A., Ghisellini G., 2002, A&A, 393, 409
 Ghirlanda G., Ghisellini G., Celotti A., 2004, A&A, 422, L55

- Ghirlanda G., Ghisellini G., Firmani C., 2006, *New Journal of Physics*, 8, 123
- Ghirlanda G., Nava L., Ghisellini G., Celotti A., Firmani C., 2009, *A&A*, 496, 585
- Ghirlanda G., Nava L., Ghisellini G., 2010, *A&A*, 511, A43
- Ghirlanda G., Ghisellini G., Nava L., 2011, *MNRAS*, 418, L109
- Ghirlanda G., Ghisellini G., Nava L., Burlon D., 2011, *MNRAS*, 410, L47
- Ghirlanda G., et al., 2012, *MNRAS*, 422, 2553
- Golenetskii S., et al., 2012, GCN 13736
- Gruber D., et al., 2011, *A&A*, 528, A15
- Gruber D., et al., 2014, *ApJS*, 211, 12
- Guiriec S., et al., 2010, *ApJ*, 725, 225
- Guiriec S., et al., 2013, *ApJ*, 770, 32
- Hjorth J., Bloom J. S., 2012, *The Gamma-Ray Burst - Supernova Connection*. pp 169–190
- Isobe T., Feigelson E. D., Akritas M. G., Babu G. J., 1990, *ApJ*, 364, 104
- J. O., et al., 2010, GCN 11089
- Kocevski D., 2012, *ApJ*, 747, 146
- Kouveliotou C., Meegan C. A., Fishman G. J., Bhat N. P., Briggs M. S., Koshut T. M., Paciesas W. S., Pendleton G. N., 1993, *ApJ*, 413, L101
- Kruehler T., et al., 2010a, GCN 14264
- Kruehler T., et al., 2010b, GCN 14500
- Krühler T., et al., 2011, *A&A*, 534, A108
- Levan A., et al., 2009, GCN 9958
- Malesani D., et al., 2009, GCN 9942
- Margutti R., et al., 2013, *MNRAS*, 428, 729
- Mészáros P., 2006, *Reports on Progress in Physics*, 69, 2259
- Milne P., et al., 2011, GCN 11708
- Nakar E., Piran T., 2002, *MNRAS*, 330, 920
- Nakar E., Piran T., 2005, *MNRAS*, 360, L73
- Nappo F., Ghisellini G., Ghirlanda G., Melandri A., Nava L., Burlon D., 2014, arXiv:1405.3981
- Nava L., et al., 2012, *MNRAS*, 421, 1256
- Nava L., Ghirlanda G., Ghisellini G., Celotti A., 2011a, *MNRAS*, 415, 3153
- Nava L., Ghirlanda G., Ghisellini G., Celotti A., 2011b, *A&A*, 530, A21
- Norris J. P., Marani G. F., Bonnell J. T., 2000, *ApJ*, 534, 248
- Perley D. A., Modjaz M., Morgan A. N., Cenko S. B., Bloom J. S., Butler N. R., Filippenko A. V., Miller A. A., 2012, *ApJ*, 758, 122
- Preece R., et al., 2014, *Science*, 343, 51
- Press W. H., Teukolsky S. A., Vetterling W. T., Flannery B. P., 2007, *Numerical recipes: the art of scientific computing* (3rd edition)
- Prochaska J., et al., 2008, GCN 8083
- Rau A., et al., 2013, GCN 15330
- Salvaterra R., Campana S., Vergani S. D., Covino S., D’Avanzo P., Fugazza D., Ghirlanda G., Ghisellini G., Melandri A., Nava L., Sbarufatti B., Flores H., Piranomonte S., Tagliaferri G., 2012, *ApJ*, 749, 68
- Shahmoradi A., Nemiroff R. J., 2011, *MNRAS*, 411, 1843
- Smette A., et al., 2013, GCN 14848
- Sparre M., et al., 2011, GCN 11607
- Tanvir N., et al., 2010, GCN 11230
- Tanvir N., et al., 2011, GCN 12225
- Tanvir N., et al., 2012a, GCN 13441
- Tanvir N., et al., 2012b, GCN 14009
- Tello J., et al., 2012, GCN 13118
- Thoene C., et al., 2008, GCN 8058
- von Kienlin A., et al., 2014, *ApJS*, 211, 13
- Wiersema K., et al., 2009, GCN 10263
- Xu D., et al., 2009, GCN 10053
- Xu D., et al., 2012, GCN 13460
- Xu D., et al., 2013a, GCN 15450
- Xu D., et al., 2013b, GCN 15645
- Yonetoku D., Murakami T., Nakamura T., Yamazaki R., Inoue A. K., Ioka K., 2004, *ApJ*, 609, 935
- Zhang F.-W., Shao L., Yan J.-Z., Wei D.-M., 2012, *ApJ*, 750, 88

APPENDIX A: RESULTS OF SPECTRAL ANALYSIS

APPENDIX B: COMPARISON WITH GRUBER ET AL. (2014) RESULTS

In this section we compare the results of our *short* and *whole* analysis to those of Gruber et al. (2014), for the bursts present in both samples. In Fig. B1 we compare the values of the low energy spectral index α (upper panel), the observed νF_ν peak energy (middle panel) and the fluence estimated in the 10 keV–1 MeV (observer frame) energy range (lower panel).

The large discrepancies found in the α parameter for GRB 080810 (ID 5) and in the observed peak energy GRB 091208B (ID 25) are likely related to the very high background contamination. The discrepancy in fluence for GRB 080916A (ID 6) is due to the different value of the β parameter used in Gruber et al. (2014). Also this burst is significantly background dominated.

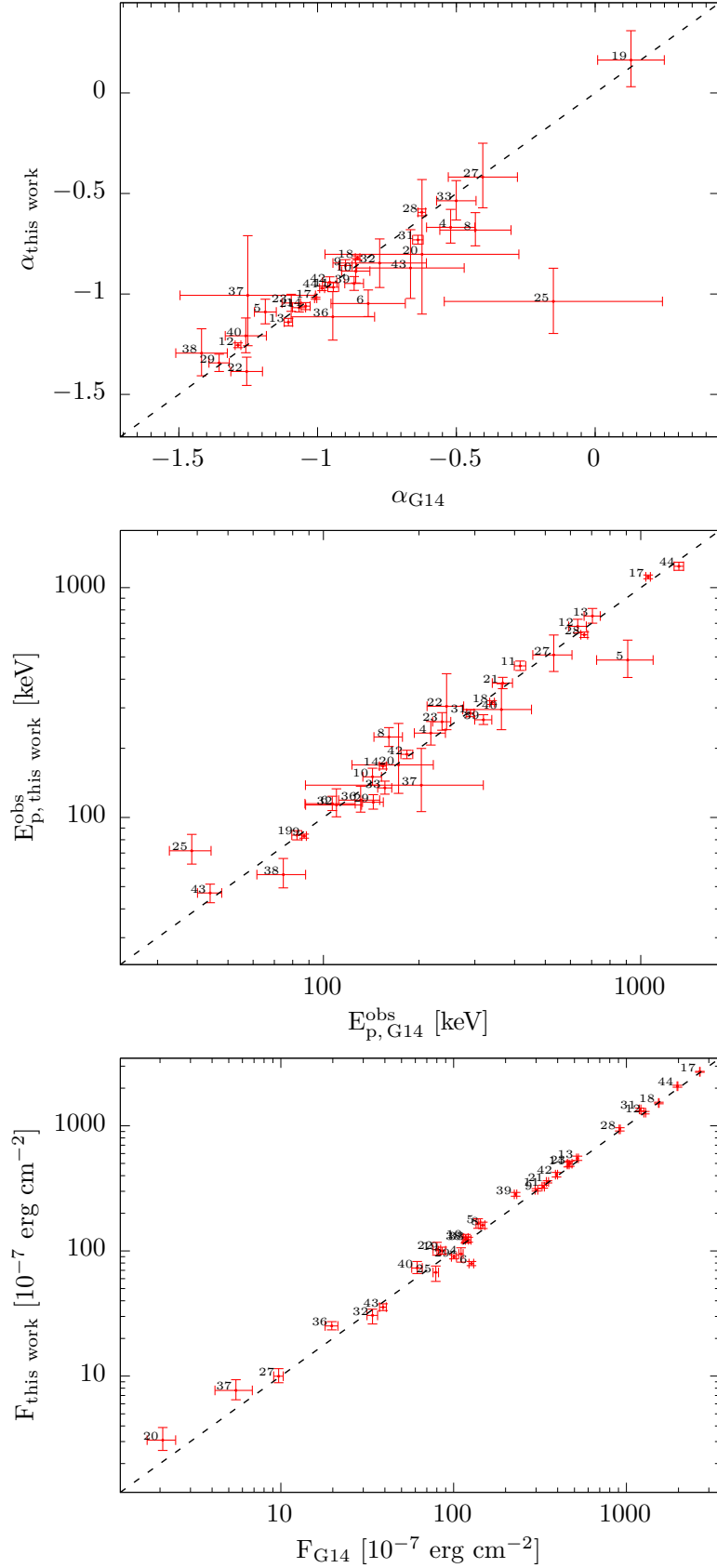


Figure B1. Comparison of the results of our *short* and *whole* analysis to those of Gruber et al. (2014), for the bursts present in both samples. Upper panel: low energy spectral index α . Middle panel: observed νF_{ν} peak energy. Lower panel: fluence estimated in the 10 keV–1 MeV (observer frame) energy range. The dashed line are the 1:1 lines.

Table A1. List of GRBs considered in this work. Columns are: [1] GRB identifier; [2] GRB name [3] fraction of day of trigger time; [4] redshift; [5] T_{90} duration in the *Fermi*/GBM 50–300 keV energy range (observer frame) *Fermi*/GBM (von Kienlin et al. 2014); [6] list of detectors used for spectral analysis; [7] background time selection; [8] redshift reference. Rows with missing data refer to short GRBs in the D14 sample (D’Avanzo et al. 2014).

ID	GRB	(day frac.)	Redshift	T_{90} [s]	Detectors	Background time sel. [s]	Redshift ref.
1	051221A		0.5465				
2	070714B		0.92				
3	080123		0.495				
4	080804	972	2.2045	24.704	n6, n7, b1	-100:-10, 50:200	Thoene et al. (2008)
5	080810	549	3.35	107.46	n7, n8, nb, b1	-100:-20, 110:200	Prochaska et al. (2008)
6	080916A	406	0.689	46.337	n7, n8, b1	-100:-20, 100:200	Fynbo et al. (2008)
7	081109	293	0.9787	58.369	n9, na, b1	-100:-20, 40:200	Krühler et al. (2011)
8	081121	858	2.512	41.985	na, nb, b1	-100:-10, 50:200	Berger & M. Rauch (2008)
9	081221	681	2.26	29.697	n1, n2, b0	-100:-10, 100:200	Salvaterra et al. (2012)
10	081222	204	2.77	18.88	n0, n1, b0	-200:-10, 50:200	Cucchiara et al. (2008)
11	090102	122	1.547	26.624	na, nb, b1	-100:-20, 50:200	de Ugarte Postigo et al. (2009)
12	090323	002	3.57	135.17	n9, nb, b1	-100:-20, 200:300	Chornock et al. (2009a)
13	090328	401	0.736	61.697	n6, n7, b1	-100:-10, 100:200	Cenko et al. (2009a)
14	090424	592	0.544	14.144	n7, n8, nb, b1	-100:-5, 100:200	Chornock et al. (2009b)
15	090510		0.903				
16	090618	353	0.54	112.39	n4, b0	-100:-20, 200:400	Cenko et al. (2009b)
17	090902	462	1.822	19.328	n0, n1, b0	-100:-10, 60:150	Cucchiara et al. (2009a)
18	090926A	181	2.1062	13.76	n6, n7, b1	-55:-10, 60:200	Malesani et al. (2009)
19	090926B	914	1.24	55.553	n7, n8, nb, b1	-100:-5, 60:200	Fynbo et al. (2009)
20	090927	422	1.37	0.512	n2, n9, na, b1	-100:-20, 10:200	Levan et al. (2009)
21	091003	191	0.8969	20.224	n3, n6, b1	-100:-10, 50:200	Cucchiara et al. (2009b)
22	091020A	900	1.71	24.256	n2, n5, b0	-100:-15, 50:200	Xu et al. (2009)
23	091024	372	1.092	93.954	n7, n8, b1	-100:-10, 60:200	Cucchiara et al. (2009c)
23	091024	380	1.092	93.954	n6, n9, b1	-200:-40, 60:200, 500:700	Cucchiara et al. (2009c)
24	091127	976	0.49	8.701	n6, n7, n9, b1	-100:-5, 30:200	Cucchiara et al. (2009d)
25	091208B	410	1.063	12.48	n9, na, b1	-100:-20, 130:250	Wiersema et al. (2009)
26	100117A		0.92				
27	100206	563	0.4068	0.128	n0, n3, b0	-100:-5, 5:200	Perley et al. (2012)
28	100414	097	1.368	26.497	n7, n9, nb, b1	-100:-20, 110:200	Cucchiara et al. (2010)
29	100615A	083	1.398	37.377	n6, n7, n8, b1	-100:-5, 100:200	Kruehler et al. (2010a)
30	100625A		0.452				
31	100728A	095	1.567	165.38	n0, n1, b0	-100:-20, 300:500	Kruehler et al. (2010b)
32	100728B	439	2.106	10.24	n6, n7, n8, b1	-100:-10, 10:200	Flores et al. (2010)
33	100814A	160	1.44	150.53	n7, n8, b1	-100:-20, 90:120, 200:300	J. et al. (2010)
34	100906A	576	1.727	110.59	nb, b1	-100:-10, 150:250	Tanvir et al. (2010)
35	101219A		0.718				
36	110106B	893	0.618	35.521	n9, na, nb, b1	-100:-20, 40:200	Chornock et al. (2011)
37	110128A	073	2.339	12.16	n6, n7, n9, b1	-100:-10, 10:200	Sparre et al. (2011)
38	110213A	220	1.46	34.305	n3, n4, b0	-100:-10, 50:200	Milne et al. (2011)
39	110731A	465	2.83	7.485	n0, n3, b0	-100:-5, 20:200	Tanvir et al. (2011)
40	110818A	860	3.36	67.073	n7, n8, nb, b1	-100:-20, 50:200	D’Avanzo et al. (2011)
41	111117A		1.3				
42	120119A	170	1.728	55.297	n9, nb, b1	-100:-20, 100:200	Cucchiara et al. (2012)
43	120326A	056	1.798	11.776	n0, n1, n2, b0	-100:-10, 20:200	Tello et al. (2012)
44	120711A	115	1.405	44.033	n2, na, b0	-100:-20, 10:50, 150:250	Tanvir et al. (2012a)
45	120712A	571	4.1745	22.528	n6, n7, b1	-100:-10, 30:200	Xu et al. (2012)
46	120716A	712	2.486	234.5	n9, na, b1	-100:-10, 20:160, 250:400	D’Elia et al. (2012)
47	120909A	070	3.93	112.07	n7, n8, b1	-100:-10, 150:300	Golenetskii et al. (2012)
48	121128A	212	2.2	17.344	n3, n4, b0	-100:-5, 50:200	Tanvir et al. (2012b)
49	130427A	324	0.3399	138.24	n9, na, b1	-200:-10	Flores et al. (2013)
50	130518A	580	2.488	48.577	n3, n7, b0, b1	-100:-20, 100:200	Cucchiara et al. (2013)
51	130603B		0.356				
52	130610A	133	2.092	21.76	n7, n8, b1	-100:-40, 30:200	Smette et al. (2013)
53	131004A	904	0.717	1.152	n9, na, b1	-100:-5, 10:200	Chornock et al. (2013)
54	131011A	741	1.874	77.057	n7, n9, nb, b1	-100:-20, 100:200	Rau et al. (2013)
55	131105A	087	1.686	112.64	n6, n7, b1	-200:-20, 150:300	Xu et al. (2013a)
56	131108A	862	2.4	18.496	n0, n3, b0	-200:-10, 50:200	de Ugarte Postigo et al. (2013)
57	131231A	198	0.642	31.232	n0, n3, b1	-100:-20, 100:200	Xu et al. (2013b)

Table A2. List of intrinsic (rest frame) spectral quantities for our GRB sample. Columns are: [1] GRB identifier; [2] GRB name; [3] Time selection (observer frame) [4] analysis specification; [5] spectral model; [6] α spectral index; [7] β spectral index spectral; [8] $\log E_p$; [9] $\log E_{iso}$ in the 1 keV–10 MeV energy range; [10] value of the Cash fit statistic and [11] degrees of freedom.

ID	GRB	Time sel. [s]		Analysis	Model	Alpha	Beta	$\log E_p$ [keV]	$\log E_{iso}$ [erg]	C-STAT	DOF
1	051221A			(short D14)		$-1.08^{+0.13}_{-0.13}$		$2.793^{+0.081}_{-0.099}$	$51.420^{+0.051}_{-0.058}$		0
2	070714B			(short D14)		$-0.86^{+0.10}_{-0.10}$		$3.33^{+0.17}_{-0.29}$	$51.991^{+0.094}_{-0.121}$		0
3	080123			(short D14)		$-1.20^{+0.38}_{-0.38}$		> 2.02	> 50.11		0
4	080804	-0.6	0.361	(first)	Band	$-0.25^{+0.64}_{-0.44}$	-2.3^a	$2.85^{+0.18}_{-0.12}$	$51.765^{+0.080}_{-0.069}$	408.58	362
		-1.024	22.528	(whole)	Band	$-0.669^{+0.089}_{-0.078}$	$-2.5^{+0.3}_{-1.1}$	$2.873^{+0.051}_{-0.052}$	$53.123^{+0.049}_{-0.065}$	510.38	361
5	080810	-1	0.305	(first)	CPL	$-0.71^{+0.29}_{-0.23}$		$3.22^{+0.18}_{-0.13}$	$52.128^{+0.107}_{-0.093}$	501.83	482
		-10.24	105.47	(whole)	Band	$-1.090^{+0.063}_{-0.059}$	-2.3^a	$3.323^{+0.087}_{-0.076}$	$53.671^{+0.039}_{-0.037}$	1221	482
6	080916A	-0.2	0.307	(first)	Band	$-0.29^{+0.45}_{-0.32}$	-2.3^a	$2.90^{+0.20}_{-0.16}$	$50.957^{+0.109}_{-0.099}$	377.97	361
		-1.024	51.2	(whole)	Band	$-1.047^{+0.067}_{-0.065}$	-2.3^a	$2.288^{+0.033}_{-0.030}$	$52.042^{+0.017}_{-0.017}$	683.35	361
7	081109	-1.2	-0.606	(first)	CPL	$-1.20^{+0.75}_{-0.49}$		$2.44^{+0.62}_{-0.27}$	$50.44^{+0.24}_{-0.18}$	420.97	360
		-5.12	34.816	(whole)	CPL	$-1.22^{+0.12}_{-0.11}$		$2.529^{+0.088}_{-0.073}$	$52.148^{+0.043}_{-0.039}$	573.17	360
8	081121	0.8	1.854	(first)	CPL	$-0.88^{+0.37}_{-0.28}$		$3.11^{+0.27}_{-0.17}$	$52.01^{+0.14}_{-0.11}$	383.75	359
		0	20.48	(whole)	Band	$-0.682^{+0.087}_{-0.078}$	$-2.2^{+0.1}_{-0.2}$	$2.896^{+0.040}_{-0.042}$	$53.477^{+0.025}_{-0.027}$	439.43	358
9	081221	-0.8	0.178	(first)	Band	$0.92^{+1.17}_{-0.75}$	-2.3^a	$2.650^{+0.095}_{-0.077}$	$51.659^{+0.056}_{-0.055}$	368.91	362
		-1.024	75.776	(whole)	Band	$-0.858^{+0.029}_{-0.027}$	$-3.3^{+0.2}_{-0.2}$	$2.4321^{+0.0083}_{-0.0089}$	$53.6217^{+0.0101}_{-0.0093}$	894.98	361
10	081222	0	1.131	(first)	Band	$-0.79^{+0.12}_{-0.11}$	-2.3^a	$3.050^{+0.086}_{-0.077}$	$52.490^{+0.034}_{-0.033}$	421.53	361
		-1.024	35.84	(whole)	Band	$-0.886^{+0.063}_{-0.059}$	$-2.4^{+0.2}_{-0.2}$	$2.753^{+0.038}_{-0.036}$	$53.420^{+0.028}_{-0.031}$	429.81	360
11	090102	0	0.764	(first)	Band	$-0.69^{+0.36}_{-0.28}$	-2.3^a	$2.94^{+0.22}_{-0.15}$	$51.466^{+0.106}_{-0.086}$	372.54	359
		-1.792	36.096	(whole)	CPL	$-0.966^{+0.022}_{-0.021}$		$3.066^{+0.021}_{-0.020}$	$53.363^{+0.012}_{-0.012}$	553.16	359
12	090323	1.4	2.771	(first)	CPL	$-1.04^{+0.19}_{-0.14}$		$3.63^{+0.31}_{-0.26}$	$52.439^{+0.096}_{-0.129}$	372.58	360
		-3.072	245.76	(whole)	Band	$-1.255^{+0.012}_{-0.012}$	-2.3^a	$3.492^{+0.030}_{-0.029}$	$54.641^{+0.010}_{-0.010}$	1596.9	360
13	090328	3.8	4.321	(first)	CPL	$-1.009^{+0.102}_{-0.091}$		$3.13^{+0.13}_{-0.11}$	$51.328^{+0.076}_{-0.069}$	433.47	361
		-4.096	78.848	(whole)	CPL	$-1.140^{+0.019}_{-0.019}$		$3.116^{+0.033}_{-0.031}$	$53.036^{+0.018}_{-0.017}$	754.48	361
14	090424	-0.2	0.263	(first)	Band	$-0.90^{+0.20}_{-0.16}$	$-2.6^{+0.3}_{-0.6}$	$2.136^{+0.062}_{-0.071}$	$50.724^{+0.064}_{-0.060}$	574.44	480
		-1.024	59.392	(whole)	Band	$-1.060^{+0.017}_{-0.017}$	$-2.8^{+0.2}_{-0.3}$	$2.412^{+0.013}_{-0.013}$	$52.637^{+0.018}_{-0.020}$	951.52	480
15	090510			(short D14)		$-0.820^{+0.020}_{-0.020}$	$-2.8^{+0.3}_{-0.3}$	$3.908^{+0.031}_{-0.033}$	$52.871^{+0.018}_{-0.019}$		0
16	090618	-0.8	-0.338	(first)	CPL	$-0.29^{+0.66}_{-0.35}$		$3.18^{+0.19}_{-0.20}$	$50.93^{+0.15}_{-0.16}$	245.72	240
		-1.024	174.08	(whole)	Band	$-1.166^{+0.013}_{-0.012}$	$-2.51^{+0.05}_{-0.05}$	$2.3981^{+0.0097}_{-0.0100}$	$53.4013^{+0.0074}_{-0.0075}$	1493.4	239
17	090902	-0.4	0.447	(first)	Band	$-0.29^{+0.17}_{-0.15}$	-2.3^a	$2.974^{+0.055}_{-0.045}$	$52.074^{+0.039}_{-0.036}$	376.4	362
		-1.024	55.296	(whole)	Band	$-1.0214^{+0.0050}_{-0.0047}$	-2.3^a	$3.4976^{+0.0079}_{-0.0082}$	$54.5667^{+0.0038}_{-0.0040}$	1879.8	362
18	090926A	0	0.932	(first)	Band	$-0.69^{+0.21}_{-0.17}$	-2.3^a	$2.95^{+0.12}_{-0.10}$	$52.050^{+0.057}_{-0.053}$	391.41	362
		-7.168	51.2	(whole)	Band	$-0.821^{+0.010}_{-0.010}$	$-2.49^{+0.06}_{-0.07}$	$2.9924^{+0.0082}_{-0.0082}$	$54.3125^{+0.0061}_{-0.0064}$	973.28	361
19	090926B	0.6	1.272	(first)	CPL	$1.2^{+2.0}_{-1.1}$		$2.564^{+0.093}_{-0.073}$	$50.827^{+0.089}_{-0.092}$	527.49	482
		-1.024	55.296	(whole)	Band	$0.16^{+0.15}_{-0.13}$	$-2.9^{+0.2}_{-0.3}$	$2.273^{+0.020}_{-0.020}$	$52.634^{+0.028}_{-0.028}$	684.57	481
20	090927	-0.256	0.448	(short)	CPL	$-0.80^{+0.37}_{-0.30}$		$2.60^{+0.18}_{-0.12}$	$51.193^{+0.101}_{-0.082}$	523.39	482
21	091003	0	0.569	(first)	Band	$-1.112^{+0.082}_{-0.075}$	-2.3^a	$3.19^{+0.15}_{-0.12}$	$51.616^{+0.061}_{-0.054}$	382.73	362
		-1.024	32.768	(whole)	Band	$-1.068^{+0.022}_{-0.021}$	-2.3^a	$2.863^{+0.025}_{-0.024}$	$53.0331^{+0.0092}_{-0.0090}$	501.81	362
22	091020A	-0.2	0.613	(first)	CPL	$-1.08^{+0.17}_{-0.15}$		$2.87^{+0.14}_{-0.11}$	$51.668^{+0.074}_{-0.065}$	381.4	362
		-6.144	45.056	(whole)	CPL	$-1.386^{+0.072}_{-0.069}$		$2.92^{+0.14}_{-0.10}$	$52.952^{+0.058}_{-0.045}$	473.64	362
23	091024	2.4	3.028	(prec.)	CPL	$-0.62^{+0.30}_{-0.25}$		$2.84^{+0.16}_{-0.12}$	$51.216^{+0.106}_{-0.088}$	390.51	360
		5	5.628	(prec.)	Band	$-0.80^{+0.86}_{-0.44}$	-2.3^a	> 2.24	> 51.16	381.46	363
24	091127	-0.2	0.247	(first)	Band	$-0.56^{+0.20}_{-0.17}$	$-2.11^{+0.07}_{-0.09}$	$2.069^{+0.058}_{-0.056}$	$51.000^{+0.036}_{-0.037}$	492.47	481
		-1.024	15.36	(whole)	Band	$-1.252^{+0.067}_{-0.063}$	$-2.21^{+0.02}_{-0.02}$	$1.706^{+0.018}_{-0.018}$	$52.2153^{+0.0076}_{-0.0076}$	713.48	481
25	091208B	-0.6	0.019	(first)	CPL	$-0.83^{+0.59}_{-0.43}$		$2.65^{+0.36}_{-0.16}$	$50.76^{+0.19}_{-0.12}$	415.97	359
		-1.024	66.56	(whole)	Band	$-0.92^{+0.17}_{-0.17}$	$-2.6^{+0.2}_{-2.5}$	$2.172^{+0.071}_{-0.050}$	$52.376^{+0.049}_{-0.077}$	837.99	358
26	100117A			(short D14)		$-0.15^{+0.21}_{-0.21}$		$2.740^{+0.062}_{-0.073}$	$50.908^{+0.051}_{-0.057}$		0
27	100206	-0.1	0.2	(short)	CPL	$-0.42^{+0.17}_{-0.15}$		$2.855^{+0.087}_{-0.072}$	$50.669^{+0.060}_{-0.053}$	399.21	362
28	100414	0.4	1.11	(first)	Band	$-0.42^{+0.23}_{-0.19}$	-2.3^a	$3.14^{+0.12}_{-0.10}$	$51.794^{+0.072}_{-0.064}$	461.74	479
		-1.024	62.464	(whole)	Band	$-0.594^{+0.017}_{-0.017}$	$-3.5^{+0.4}_{-0.7}$	$3.169^{+0.012}_{-0.012}$	$53.773^{+0.012}_{-0.013}$	1109.4	478
29	100615A	-0.2	0.519	(first)	CPL	$-0.82^{+0.15}_{-0.13}$		$3.17^{+0.16}_{-0.15}$	$51.65^{+0.11}_{-0.10}$	498.68	485
		-1.024	39.936	(whole)	CPL	$-1.343^{+0.044}_{-0.043}$		$2.446^{+0.033}_{-0.030}$	$52.727^{+0.016}_{-0.015}$	783.08	485
30	100625A			(short D14)		$-0.60^{+0.11}_{-0.11}$		$2.846^{+0.066}_{-0.078}$	$50.875^{+0.017}_{-0.018}$		0
31	100728A	3.6	4.37	(first)	Band	$-0.54^{+0.57}_{-0.35}$	-2.3^a	> 3.02	> 51.67	381.15	362
		-4.096	278.53	(whole)	Band	$-0.730^{+0.022}_{-0.021}$	$-2.13^{+0.04}_{-0.05}$	$2.863^{+0.015}_{-0.015}$	$54.084^{+0.011}_{-0.011}$	3289.9	361

Table A2 – *continued*

ID	GRB	Time sel. [s]			Model	Alpha	Beta	$\log E_p$ [keV]	$\log E_{\text{iso}}$ [erg]	C-STAT	DOF
32	100728B	-1.2	-0.268	(first)	Band	-0.84 ^{+0.35} _{-0.29}	-2.3 ^a	2.74 ^{+0.24} _{-0.15}	51.516 ^{+0.124} _{-0.092}	592.61	484
		-1.024	7.168	(whole)	Band	-0.85 ^{+0.12} _{-0.12}	-2.3 ^{+0.2} _{-0.4}	2.547 ^{+0.070} _{-0.052}	52.610 ^{+0.050} _{-0.068}	561.66	483
33	100814A	-0.6	0.132	(first)	CPL	-0.58 ^{+0.37} _{-0.27}		3.09 ^{+0.24} _{-0.19}	51.48 ^{+0.17} _{-0.14}	393.97	359
		-1.152	152.45	(whole)	CPL	-0.536 ^{+0.100} _{-0.095}		2.516 ^{+0.029} _{-0.027}	52.831 ^{+0.020} _{-0.019}	737.63	359
34	100906A	0.2	1.018	(first)	CPL	-1.03 ^{+0.14} _{-0.21}		3.25 ^{+0.62} _{-0.17}	52.12 ^{+0.24} _{-0.10}	262	238
		0	120.83	(whole)	Band	-1.307 ^{+0.078} _{-0.068}	-2.00 ^{+0.08} _{-0.18}	> 2.44	> 53.45	864.42	237
35	101219A	(short D14)				-0.22 ^{+0.27} _{-0.27}		2.925 ^{+0.073} _{-0.088}	51.688 ^{+0.057} _{-0.065}		0
36	110106B	-1	-0.515	(first)	Band	-0.83 ^{+0.77} _{-0.43}	-2.3 ^a	> 2.31	> 50.56	541.31	480
		-2.048	18.432	(whole)	CPL	-1.11 ^{+0.13} _{-0.12}		2.284 ^{+0.061} _{-0.052}	51.438 ^{+0.034} _{-0.032}	538.47	480
37	110128A	-2.2	-1.198	(first)	CPL	-0.61 ^{+0.66} _{-0.46}		2.80 ^{+0.29} _{-0.18}	51.37 ^{+0.17} _{-0.13}	506.37	484
		-2.048	9.216	(whole)	CPL	-1.01 ^{+0.30} _{-0.25}		2.66 ^{+0.16} _{-0.12}	52.032 ^{+0.086} _{-0.075}	477.39	484
38	110213A	-3.072	35.84	(whole)	Band	-1.29 ^{+0.12} _{-0.11}	-2.13 ^{+0.06} _{-0.08}	2.142 ^{+0.070} _{-0.058}	52.983 ^{+0.024} _{-0.025}	471.04	360
39	110731A	-0.8	0.349	(first)	CPL	-1.27 ^{+0.15} _{-0.14}		2.665 ^{+0.068} _{-0.058}	52.355 ^{+0.040} _{-0.037}	400.95	360
		-1.024	13.312	(whole)	Band	-0.951 ^{+0.035} _{-0.034}	-2.7 ^{+0.2} _{-0.3}	3.015 ^{+0.022} _{-0.021}	53.777 ^{+0.015} _{-0.017}	501.5	359
40	110818A	-0.6	0.708	(first)	Band	-0.79 ^{+2.76} _{-0.55}	-2.3 ^a	> 2.34	> 51.95	479.49	481
		-7.168	45.056	(whole)	CPL	-1.208 ^{+0.089} _{-0.084}		3.109 ^{+0.113} _{-0.088}	53.292 ^{+0.052} _{-0.044}	714.43	481
41	111117A	(short D14)				-0.28 ^{+0.28} _{-0.28}		2.98 ^{+0.12} _{-0.18}	51.53 ^{+0.12} _{-0.16}		0
42	120119A	-0.2	0.618	(first)	CPL	-1.30 ^{+0.92} _{-0.25}		2.97 ^{+0.62} _{-0.53}	51.27 ^{+0.23} _{-0.28}	393.34	360
		-2.048	57.344	(whole)	Band	-0.941 ^{+0.027} _{-0.025}	-2.5 ^{+0.1} _{-0.2}	2.710 ^{+0.018} _{-0.019}	53.568 ^{+0.018} _{-0.018}	834.93	359
43	120326A	-1	-0.161	(first)	CPL	-1.05 ^{+0.27} _{-0.24}		2.379 ^{+0.102} _{-0.080}	51.301 ^{+0.062} _{-0.057}	514.08	483
		-2.048	13.312	(whole)	Band	-0.87 ^{+0.19} _{-0.15}	-2.5 ^{+0.1} _{-0.2}	2.118 ^{+0.038} _{-0.043}	52.546 ^{+0.027} _{-0.027}	568.22	482
44	120711A	0.2	0.921	(prec.)	CPL	-0.35 ^{+0.52} _{-0.38}		3.02 ^{+0.14} _{-0.11}	51.528 ^{+0.101} _{-0.093}	368.65	362
		61	61.722	(first)	CPL	-0.93 ^{+0.63} _{-0.19}		3.45 ^{+0.25} _{-0.53}	51.72 ^{+0.14} _{-0.34}	398.14	362
		-1.024	117.76	(whole)	Band	-0.972 ^{+0.011} _{-0.011}	-3.1 ^{+0.2} _{-0.2}	3.474 ^{+0.018} _{-0.017}	54.2786 ^{+0.0079} _{-0.0079}	666.6	361
45	120712A	-1.4	0.152	(first)	Band	-1.25 ^{+0.45} _{-0.28}	-2.3 ^a	> 2.97	> 52.27	420.97	362
		-1.4	16	(whole)	Band	-0.62 ^{+0.20} _{-0.20}	-1.88 ^{+0.09} _{-0.14}	> 2.81	> 53.30	468.5	361
46	120716A	-0.8	0.246	(prec.)	Band	-0.58 ^{+0.21} _{-0.19}	-2.3 ^a	2.900 ^{+0.081} _{-0.068}	52.043 ^{+0.045} _{-0.042}	376.43	361
		177	178.046	(first)	Band	-0.58 ^{+0.23} _{-0.20}	-2.3 ^a	3.008 ^{+0.103} _{-0.086}	52.092 ^{+0.049} _{-0.046}	403.41	361
		177	235	(whole)	Band	-1.077 ^{+0.061} _{-0.058}	-2.7 ^{+0.2} _{-0.8}	2.660 ^{+0.036} _{-0.034}	53.325 ^{+0.030} _{-0.037}	461.22	360
47	120909A	-1.6	-0.121	(first)	CPL	-0.76 ^{+0.24} _{-0.19}		3.68 ^{+0.26} _{-0.22}	52.46 ^{+0.11} _{-0.14}	376.75	360
		-1.6	130	(whole)	Band	-1.039 ^{+0.063} _{-0.059}	-2.2 ^{+0.1} _{-0.2}	2.941 ^{+0.049} _{-0.045}	53.818 ^{+0.029} _{-0.031}	1086.8	359
48	121128A	2	2.96	(first)	Band	-0.43 ^{+0.21} _{-0.19}	-2.3 ^a	2.596 ^{+0.054} _{-0.047}	52.099 ^{+0.028} _{-0.027}	366.13	360
		-0.6	28	(whole)	Band	-0.892 ^{+0.116} _{-0.095}	-2.6 ^{+0.1} _{-0.2}	2.315 ^{+0.028} _{-0.033}	53.123 ^{+0.024} _{-0.024}	491.99	359
49	130427A	0	0.402	(first)	Band	-0.399 ^{+0.026} _{-0.025}	-3.5 ^{+0.3} _{-0.4}	3.060 ^{+0.015} _{-0.015}	51.817 ^{+0.011} _{-0.012}	405.5	359
50	130518A	13	14.046	(first)	Band	-0.74 ^{+0.25} _{-0.23}	-2.3 ^a	2.854 ^{+0.118} _{-0.084}	51.972 ^{+0.051} _{-0.046}	481.17	481
		0	75	(whole)	Band	-0.925 ^{+0.015} _{-0.014}	-2.35 ^{+0.06} _{-0.07}	3.167 ^{+0.015} _{-0.015}	54.2712 ^{+0.0055} _{-0.0056}	1128.5	480
51	130603B	(short D14)				-0.73 ^{+0.15} _{-0.15}		2.952 ^{+0.061} _{-0.071}	51.326 ^{+0.045} _{-0.050}		0
52	130610A	1.8	2.728	(first)	CPL	-0.50 ^{+0.46} _{-0.36}		2.78 ^{+0.14} _{-0.10}	51.541 ^{+0.090} _{-0.080}	340.54	360
		1.8	20	(whole)	CPL	-0.83 ^{+0.11} _{-0.11}		2.716 ^{+0.046} _{-0.042}	52.619 ^{+0.029} _{-0.027}	467.98	360
53	131004A	-0.8	0.4	(short)	Band	-0.50 ^{+2.10} _{-0.63}	-2.3 ^a	> 1.71	> 51.13	368.42	360
54	131011A	-0.4	0.462	(first)	CPL	-0.71 ^{+0.30} _{-0.22}		3.39 ^{+0.26} _{-0.21}	51.86 ^{+0.15} _{-0.15}	475.15	480
		-0.4	80	(whole)	Band	-0.997 ^{+0.168} _{-0.085}	-2.0 ^{+0.2} _{-0.3}	> 2.66	> 53.17	939.17	479
55	131105A	-0.4	0.406	(first)	CPL	-0.81 ^{+0.30} _{-0.24}		3.03 ^{+0.23} _{-0.15}	51.47 ^{+0.14} _{-0.11}	383.21	362
		-0.4	120	(whole)	CPL	-1.295 ^{+0.029} _{-0.028}		2.795 ^{+0.036} _{-0.033}	53.280 ^{+0.017} _{-0.016}	704.34	362
56	131108A	0.2	1.22	(first)	Band	-0.549 ^{+0.101} _{-0.090}	-2.1 ^{+0.1} _{-0.1}	2.933 ^{+0.049} _{-0.050}	52.872 ^{+0.022} _{-0.024}	366.2	361
		0.2	22	(whole)	Band	-0.867 ^{+0.030} _{-0.029}	-2.4 ^{+0.1} _{-0.2}	3.048 ^{+0.025} _{-0.024}	53.799 ^{+0.013} _{-0.014}	458.83	361
57	131231A	1.8	2.293	(first)	CPL	-0.046 ^{+0.839} _{-0.580}		2.418 ^{+0.128} _{-0.091}	50.256 ^{+0.093} _{-0.086}	403.2	360
		1.8	70	(whole)	Band	-1.208 ^{+0.011} _{-0.010}	-2.33 ^{+0.04} _{-0.05}	2.453 ^{+0.011} _{-0.011}	53.3352 ^{+0.0082} _{-0.0086}	1261.2	359